Supporting Information

Serero et al. 10.1073/pnas.1314423111

SI Materials and Methods

Yeast Strains and Constructions. All strains used in this study are derivatives of BY4741 (*MAT***a** *his3Δ1 leu2Δ0 met15Δ0 ura3Δ0*) (1). Gene deletions were made by PCR-based gene disruption methods using genomic DNA from the collection of the *Saccharomyces cerevisiae* single-gene deletants (2). The PCR-amplified DNA fragment, which contains the KanMX4-selectable marker flanked by the upstream and downstream sequence of each ORF of interest, was transformed into BY4741, and the gene deletions were verified by PCR and Southern blot. The double *cac1Δ cac3Δ* and triple *mec1Δ tel1Δ sml1Δ* mutant haploid were obtained by single mutant mating-type switching, crossing, sporulation, and isolation of the appropriate strains, ultimately verified by PCR. The *sml1Δ* mutation is necessary to suppress the lethality of the *mec1Δ* mutation (3); in the main text, the *mec1Δ tel1Δ sml1Δ* genotype is abbreviated to *mec1Δ tel1Δ*. Introduction of the gross chromosomal rearrangement (GCR) assay in the WT (BY4741) and derivative *pif1Δ* mutant was performed by replacing *HXT13* (~7.5 kb telomeric to *CAN1*) with a *URA3* cassette.

Production of the Mutation Accumulation Lines. In most instances (Fig. 1), four parallel mutation accumulation (MA) lines were derived from each parental strain and subjected to 75 (*mre11Δ and cac1Δ cac3Δ* mutants) or 100 (WT, *rad27Δ, pif1Δ, msh2Δ, tsa1Δ, pol32Δ,* and *clb5Δ* mutants) single-cell bottlenecks, except for the *mec1Δ tel1Δ sml1Δ* mutant whose eight derived lines were passed through 25 bottlenecks. The single-cell bottleneck was performed by picking a random average-sized colony and by streaking it for individual colony forming units on rich yeast extract/peptone/dextrose (YPD) plates for 2–4 d of growth at 30 °C.

Mutation Assays. The canavanine resistance (Can^r) and GCR assays were performed as described in refs. 4 and 5, respectively.

Next-Generation Sequencing. Genomic DNA from 44 yeast strains (four lines per strain but eight for *mec1Δ tel1Δ sml1Δ*) was sequenced using V4 and 5500 SOLiD instruments (Life Technologies) following the manufacturer's standard protocols (Life Technologies, v.4 protocol). Libraries were constructed for (50 + 35 bp) paired-end sequencing (with an insert size of ~145 bp), barcoded, and mixed in four pools: WT, *pif1Δ* and *rad27Δ* (pool 1), *msh2Δ, tsa1Δ, pol32Δ and clb5Δ* (pool 2), *mre11Δ* and *cac1Δ cac3Δ,* (pool 3), and *mec1Δ tel1Δ sml1Δ* (pool 4). On average, 8×10^7 reads per line were obtained.

Reads Mapping. Mapping of the read was performed by programs provided by Life Technologies. For SNP calling in the unique regions, small InDel calling, and calling of intermediate-sized and large structural variants, nonredundant reads were aligned with the BioScope (v.1.3) and LifeScope (2.5) (Life Technologies). For SNP calling in the multialigned (M) regions and identification of structural variations, the reads were aligned with mapreads from corona-lite4.2.2 (Life Technologies). Intragenomic repetitive DNA such as Ty elements and multigene families affect the accuracy of the read alignment and are a source of false-positive mutation calls. Before mutation analysis, we identified the uniquely (U) and multialigned (M) regions across the reference genome of *S. cerevisiae* by analyzing multialignments from high-throughput sequencing simulation (HTS simulation). The coverage calculation was performed on the U regions. After removal of the PCR duplicates (average, 25%), it varies between ~75× and 153× (average, ~105×). The reads were mapped on the S288c reference genome, version June 2008 (S288C_reference_genome_R61-1–1_20080605, SGD *Saccharomyces* Genome Database; www.yeastgenome.org/). Then, the LiftOver Genome Annotations tool (6) (http://genome.ucsc.edu/cgi-bin/hgLiftOver) was used to convert mutation coordinates from the S288C genome version of June 2008 to the version of February 2011 (S288C_reference_genome_R64-1–1_20110203, SGD *Saccharomyces* Genome Database; www.yeastgenome.org/).

Bioinformatics Methods of Mutation Calling and Molecular Validations. An extensive set of bioinformatics pipelines, diagrammed in Fig. S1, was used to detect all mutation types. Sequence variations recurrently found in the MA lines, thus corresponding to constitutive variations between the reference S288C genome and the BY4741 strain background, were discarded.

Base substitution (SNP) calling in the U regions was performed with BioScope (v1.3). In addition to default parameters, the following rules were applied: (*i*) calls should be detected on both DNA strands, (*ii*) only unique reads were used for SNP calling, (*iii*) adjacent SNPs should be detected, (*iv*) the values for Reads Max Mismatch Alignmentlength and Reads Min Alignmentlength Readlength ratios were set to 0.5, and (*v*) high stringency criteria were applied. Finally, generated calls were considered robust if they were reported in at least 70% of the reads covering the SNP position. Differently, SNP calling in the M regions, was performed by using adjacent unique sequence variations defined by the HTS simulation. SNP calls were made by analysis of base changes in 50-bp read alignments with AnnotateChanges (v0.2, corona-1.0.1r0-4) provided by ABI (Life Technologies). A call was selected if the base change was consistent with a minimal of 10 read alignments on each strand with a minimal of five different alignment starting points. Within the M regions, calls within homopolymers and microsatellites tracts remained difficult to ascertain and therefore were eliminated.

Small InDel calls (−11 to +3 bp) were performed in the U regions with the BioScope v1.3 software using the default values. Calls supported by at least six nonredundant reads and by at least three reads on each strand were retained.

Annotation of the SNP and small InDel mutations were determined by the Variant Effect Predictor tool (7) (www.ensembl.org/tools.html).

The various structural variants (SVs) were detected in the U regions from inconsistencies in paired-end read alignments identified with SVDetect (8). The coordinates of the large InDels were found by identifying significant changes in coverage along chromosomes with FREEC (9). Only unique alignments were used for FREEC analysis. Copy number variation was calculated by dividing the mean coverage of the large InDel region by the average of haploid genome coverage. Intermediate-sized and large SV calls (>50 bp) were detected with SVDetect. The size of the sliding window used for partitioning the yeast genome was defined as $\mu + 2$ SD, with μ and SD corresponding to the values of mean insert size and of the SD (both values were determined by SVDetect), respectively. Our 44 paired-end libraries had insert size varying between 116 and 188 bp. The size of the overlapping windows was fixed to be equal to half of the sliding window size. The minimal requirement for a mutational call was 20 paired-end reads.

The aneuploidies were detected by comparing the coverage of each chromosome to the coverage of the chromosome X unique regions because this chromosome did not exhibit copy number variations across all of the MA lines.

Mutation Call Validations by Comparative Genome Hybridization Array, Pulsed-Field Gel Electrophoresis, PCR Amplification, and Southern Blotting, FACS, and Sanger. Comparative genome hybridization array (aCGH) analyses were performed on whole genomic DNA extracts or purified band from pulsed-field gel electrophoresis (PFGE) electrophoresis, hybridized on whole genome Agilent Yeast ChIP-on-chip Kit 4 × 44K slides (10). SNPs and small-indels were verified by capillary sequencing (Big Dye Terminator V1.1 Cycle sequencing kit; Life Technologies) of the four MA lines of the corresponding WT or mutant strains. FACS samples (10^7 cells) of exponentially growing cultures were fixed with 70% ethanol, stained with propidium iodide, and analyzed on the flow cytometer (BD Accuri).

1. Brachmann CB, et al. (1998) Designer deletion strains derived from Saccharomyces cerevisiae S288C: A useful set of strains and plasmids for PCR-mediated gene disruption and other applications. *Yeast* 14(2):115–132.
2. Winzeler EA, et al. (1999) Functional characterization of the S. cerevisiae genome by gene deletion and parallel analysis. *Science* 285(5429):901–906.
3. Zhao X, Muller EG, Rothstein R (1998) A suppressor of two essential checkpoint genes identifies a novel protein that negatively affects dNTP pools. *Mol Cell* 2(3):329–340.
4. Tishkoff DX, Filosi N, Gaida GM, Kolodner RD (1997) A novel mutation avoidance mechanism dependent on S. cerevisiae RAD27 is distinct from DNA mismatch repair. *Cell* 88(2):253–263.
5. Chen C, Kolodner RD (1999) Gross chromosomal rearrangements in Saccharomyces cerevisiae replication and recombination defective mutants. *Nat Genet* 23(1):81–85.
6. Hinrichs AS, et al. (2006) The UCSC Genome Browser Database: Update 2006. *Nucleic Acids Res* 34(Database issue):D590–D598.
7. McLaren W, et al. (2010) Deriving the consequences of genomic variants with the Ensembl API and SNP effect predictor. *Bioinformatics* 26(16):2069–2070.
8. Zeitouni B, et al. (2010) SVDetect: A tool to identify genomic structural variations from paired-end and mate-pair sequencing data. *Bioinformatics* 26(15):1895–1896.
9. Boeva V, et al. (2011) Control-free calling of copy number alterations in deep-sequencing data using GC-content normalization. *Bioinformatics* 27(2):268–269.
10. Lundblad V, Struhl K (2010) Yeast. *Curr Protocols Molec Biol* 92:13.10.11–13.10.14.

Fig. S1. Flow diagram of the bioinformatics pipeline. First, sequence reads were mapped to the yeast S288c genome with a median read depth reaching ∼140×. Second, mutation types were identified in uniquely aligned regions using a set of bioinformatics programs: (*i*) single nucleotide variant calls (SNPs), (*ii*) small deletion (up to 11 bp) and insertion (up to 3 bp) (small InDels) calls were identified with Bioscope-v.1.3, (*iii*) intermediate-sized structural variants (SVs, from 50 bp to 5 kb) were detected with SVDetect (8), (*iv*) large structural variants (SVs); >5 kb) were identified with SVDetect and FREEC (9), and (*v*) aneuploidy and polyploidy were detected with a global coverage variation analysis. Third, a high-throughput sequencing (HTS) simulation was used to filter multi-alignments in intragenomic repetitive sequences. Finally, a subset of SNP calls found in these regions could be accurately identified and validated. Mutations identified in unique regions were classified constitutive (found in most of the lines) or acquired (found in one of the MA lines derived from the same mutator parent). Fourth, a fraction of the acquired variants (from 10% to 80%) was experimentally validated by classical molecular methods (*SI Materials and Methods*).

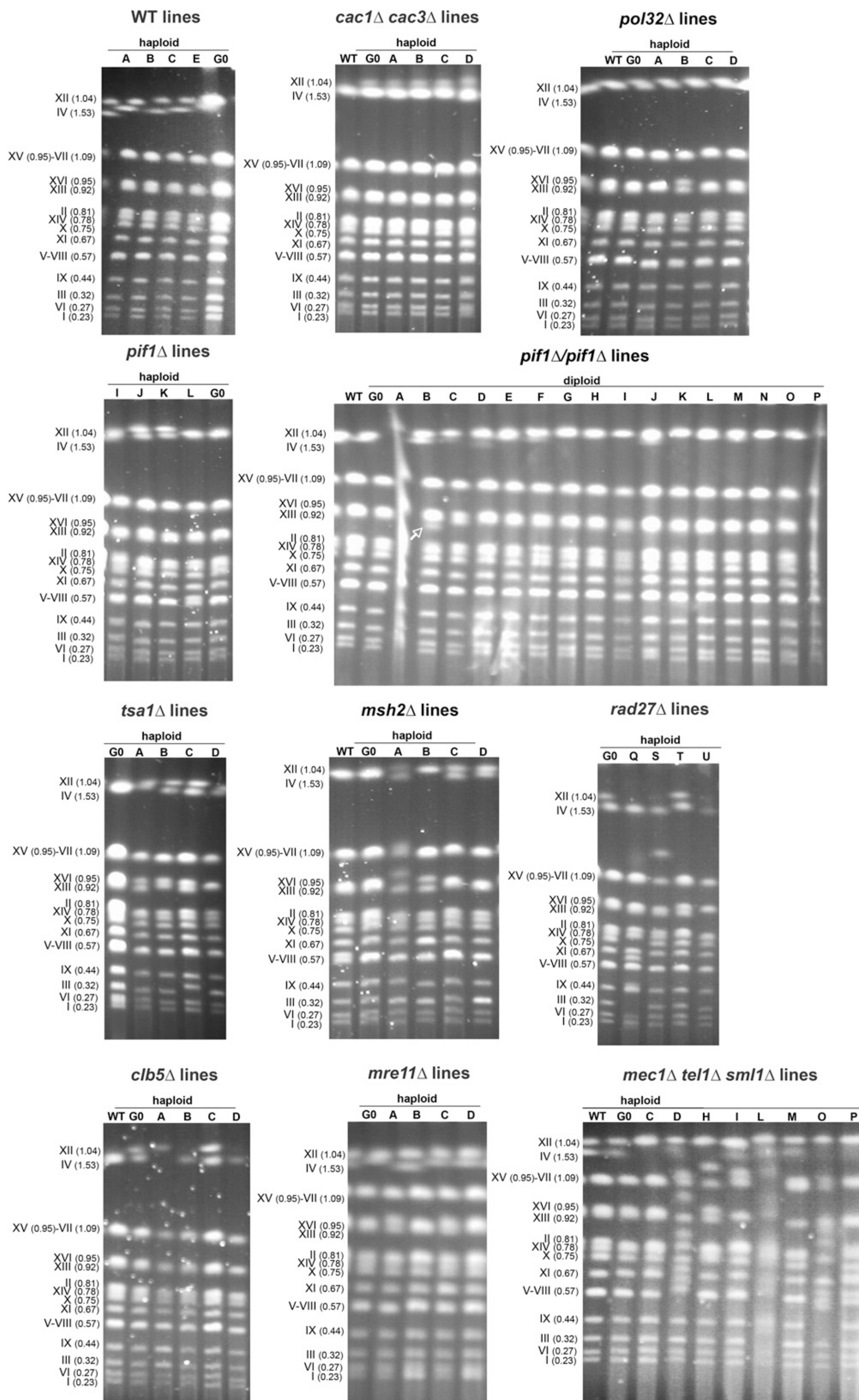

Fig. S2. PFGE analyses of haploid MA lines. For each mutant, a set of four haploid lines was subjected to 100 bottleneck passages, except the *cac1*Δ *cac3*Δ and *mre11*Δ lines (75 bottleneck passages). The eight haploid *mec1*Δ *tel1*Δ *sml1*Δ lines were passaged until 25 bottlenecks. For the *pif1*Δ mutant, an additional set of 16 homozygous diploid parallel lines were subjected to 25 bottlenecks. The letter corresponding to each line is given on the top of the panels; the mutant parental strain is indicated by G0. WT corresponds to the haploid BY4741 strain. Chromosomes indicated with arrows are discussed in Datasets S1–S10. Chromosome numbers and their expected sizes (Mb) are given on the left.

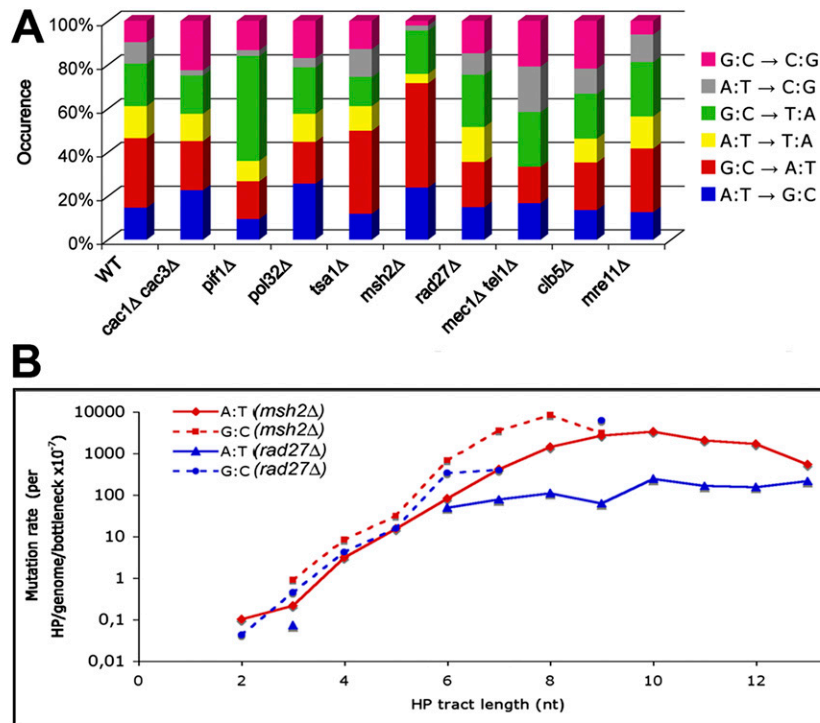

Fig. S3. Mutation profiles. (*A*) Base substitution profiles of the WT and mutant lines. The total number of mutations per strain is shown on the top. (*B*) The rate of +1/−1 InDels mutagenesis in the *msh2Δ* and *rad27Δ* lines depends on homopolymer tract length. The mutation rate was calculated on the basis of the following formula: (number of dN mutations)/(number of dN runs in the genome)/(100 bottlenecks). We determined the number of dN runs of a given length in unique regions of the genome and then calculated the number of mutations occurring in these dN runs in the four *msh2Δ* (red line) and *rad27Δ* (blue line) mutants. This calculation was performed for poly(A:T) and poly(G:C) tracts up to 14 nucleotides long. Surprisingly, no +1/−1 InDels located in poly(A) and poly (T) tracts between 4 and 5 bp long and in poly(G) and poly(C) tracts of 8 bp long were identified in the *rad27Δ* lines for a reason that remains to be elucidated.

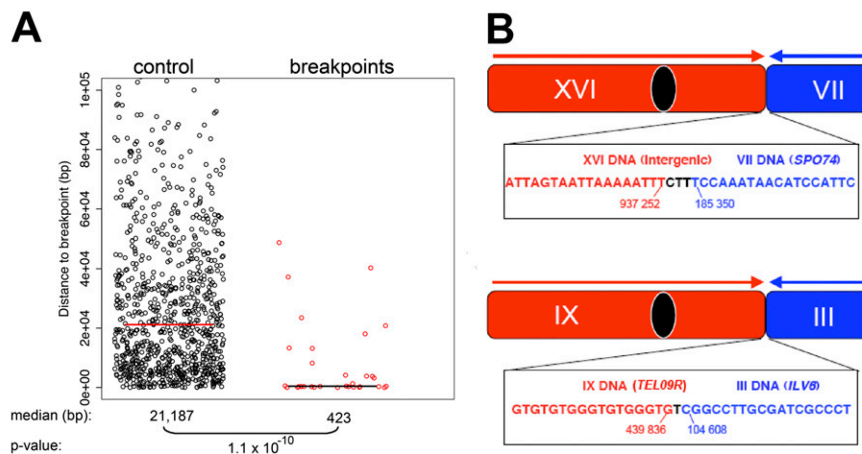

Fig. S4. Profile of chromosome rearrangement breakpoints. (*A*) Enrichment of chromosome breakpoints in the vicinity of the Ty elements. The median distance (bp) between the unique breakpoints identified in the mutant lines ($n = 33$) (*tsa1Δ, msh2Δ, rad27Δ, clb5Δ, mre11Δ* and *mec1Δ, tel1Δ sml1Δ*) and the nearest Ty and/or LTR elements was calculated. As a control, the same analysis was performed between a set of random coordinates in unique regions ($n = 918$) and the nearest Ty and/or LTR elements. The sets of random coordinates and breakpoints are represented in black and red rhombus, respectively. The *P* value was calculated with a Wilcoxon test of the median, two-tailed. (*B*) Breakpoint junction sequences of two nonreciprocal translocations identified in the *mec1Δ tel1Δ sml1Δ* lines. Panels show the structure of the translocations identified in the M (*Top*) and O lines (*Bottom*). The sequence identity between the two chromosomes at the junction is colored in black. As the sequence junctions share low homology (only up to three nucleotides), these chromosome rearrangements are likely the product of nonhomologous end joining events. The name of the gene is indicated in parentheses when the breakpoint is intragenic. *TEL09R* corresponds to the telomeric region on the right arm of chromosome IX.

Fig. S5. Characterization of a circular derivative of chromosome II identified in an *mre11Δ* line. The *mre11Δ* G_{75}-C line carries an interstitial 32-kb duplication that includes the centromere, flanked by repetitive DNA Ty and LTR elements (*A*). DNA from the *mre11Δ* G_{75}-C line was digested with SpeI and hybridized to a probe derived from chromosome II (the probe is represented by a solid rectangle in *A* and *B*). The expected DNA fragment size for a linear chromosome (12.3 kb) was found in the WT strain (lane 1), in the *mre11Δ* parental strain (lane 2), and in the 4 derived *mre11Δ* A-D lines (lanes 3–6) (*C*). An additional band of ∼15.5 kb corresponding to the expected size for a circular chromosome was only detected in the *mre11Δ* G_{75}-C line (lane 5) (*C*). The size of the band indicates that a recombined full-length Ty element is part of the junction in the *mre11Δ* G_{75}-C line.

Table S1. Rate of Can^r progeny in MA lines (G_0 and G_{100} bottlenecks)

Strain	Mutation accumulation lines*	Can^r mutation rate ($\times 10^{-7}$)	95% CI†		Fold increase‡
			Upper	Lower	
WT	G_0	2.80	0.77	2.20	1.0
	G_{100}-A	2.35	0.50	1.50	0.8
	G_{100}-B	1.62	0.37	0.77	0.6
	G_{100}-C	2.49	1.09	0.73	0.9
	G_{100}-E	3.05	0.71	1.70	1.1
cac1Δ cac3Δ	G_0	1.16	0.23	1.02	1.0
	G_{75}-A	0.82	0.26	0.77	0.7
	G_{75}-B	0.97	0.43	1.03	0.8
	G_{75}-C	0.48	0.19	0.93	0.4
	G_{75}-D	0.48	0.18	0.93	0.4
pif1Δ	G_0	20.41	7.10	8.42	1.0
	G_{100}-I	16.83	7.83	9.02	0.8
	G_{100}-J	13.38	6.77	5.72	0.7
	G_{100}-K	11.21	4.50	6.29	0.5
	G_{100}-L	7.31	3.12	4.26	0.4
pol32Δ	G_0	2.81	1.04	2.44	1.0
	G_{100}-A	2.07	0.59	0.70	0.7
	G_{100}-B	1.37	0.33	0.80	0.5
	G_{100}-C	2.81	0.99	1.44	1.0
	G_{100}-D	2.11	0.70	2.46	0.7
tsa1Δ	G_0	19.25	3.79	8.23	1.0
	G_{100}-A	22.42	9.95	5.61	1.2
	G_{100}-B	9.31	2.38	5.70	0.5
	G_{100}-C	17.00	6.99	7.64	0.9
	G_{100}-D	7.25	1.86	6.49	0.4
msh2Δ	G_0	59.60	38.19	88.17	1.0
	G_{100}-A§	ND	—	—	—
	G_{100}-B	20.21	5.40	5.97	0.3
	G_{100}-C	34.97	9.57	13.99	0.6
	G_{100}-D	66.76	27.49	3.95	1.1
rad27Δ	G_0	95.87	24.32	101.07	1.0
	G_{100}-Q§	ND	—	—	—
	G_{100}-S	126.19	57.92	160.24	1.3
	G_{100}-T	90.74	45.20	46.43	0.9
	G_{100}-U	17.91	26.02	6.30	0.2
mec1Δ tel1Δ sml1Δ	G_0	482.48	66.34	294.10	—
clb5Δ	G_0	2.28	0.85	4.72	1.0
	G_{100}-A	4.19	1.12	3.73	1.8
	G_{100}-B	1.95	0.60	1.67	0.9
	G_{100}-C§	ND	—	—	—
	G_{100}-D	2.40	0.72	2.25	1.1
mre11Δ	G_0	20.81	9.10	4.18	1.0
	G_{75}-A	24.93	6.22	4.02	1.2
	G_{75}-B	23.58	10.52	7.76	1.1
	G_{75}-C	19.73	7.43	7.30	0.9
	G_{75}-D	3.15	1.41	3.35	0.2

The CAN^r assay was performed as previously described (4). Strains are as in Table 2. ND, not determined.

*G_0 or G_{100} indicated the number of bottleneck passages, followed by the clone line (letters).

†95% CIs of the median were calculated by Luria-Delbruck fluctuation analysis (Lea Coulson Median).

‡Fold increase relative to the parental (G_0) rate.

§The CAN^r assay could not be performed because the cell line became diploid (*rad27Δ* G_{100}-Q) (Fig. 3), acquired an arginine deficiency (*msh2Δ* G_{100}-A) (Table S2), or became disomic for chromosome V that carries the *CAN1* gene (*clb5Δ* G_{100}-C) (Table S4).

Table S2. Phenotypic growth analysis of the mutation accumulation lines after bottleneck cycles

Strain	Mutation accumulation line*	Growth on YPD[†]			Growth on YPG[‡]	Growth on synthetic supplemented media[§]	Mating efficiency[¶]
		23 C°	30 °C	37 °C			
WT	G_{100}-A	+++	+++	+++	+++	+++	+++
	G_{100}-B	+++	+++	+++	+++	+++	+++
	G_{100}-C	+++	+++	+++	+++	+++	+++
	G_{100}-E	+++	+++	+++	+++	+++	+++
cac1Δ cac3Δ	G_{75}-A	+++	+++	+++	+++	+++	+++
	G_{75}-B	+++	+++	+++	+++	+++	+++
	G_{75}-C	+++	+++	+++	+++	+++	+++
	G_{75}-D	+++	+++	+++	+++	+++	+++
pif1Δ	G_{100}-I	+++	+++	+++	−	+++	+++
	G_{100}-J	+++	+++	+++	−	+++	+++
	G_{100}-K	+++	+++	+++	−	+++	+++
	G_{100}-L	+++	+++	+++	−	+++	−
pol32Δ	G_{100}-A	+++	+++	+++	+++	+++	+++
	G_{100}-B	+++	+++	+++	+++	+++	+++
	G_{100}-C	+++	+++	+++	+++	+++	+++
	G_{100}-D	+++	+++	+++	+++	+++	+++
tsa1Δ	G_{100}-A	+++	+++	+++	+++	+++	−
	G_{100}-B	−	+++	+++	−	+	+++
	G_{100}-C	−	+++	−	+++	+++	−
	G_{100}-D	+++	+++	−	+++	+++	−
msh2Δ	G_{100}-A	+	+	−	−	+, arg-	−
	G_{100}-B	+++	+	+++	−	+++, trp-	+++
	G_{100}-C	+++	+	−	−	+++	−
	G_{100}-D	+++	+	−	−	+	−
rad27Δ	G_{100}-Q	+++	+++	−	−	+++, arg-,lys-	−
	G_{100}-S	+++	+++	−	−	+++	+++
	G_{100}-T	+++	+++	+++	+	+++	+++
	G_{100}-U	+++	+++	−	−	+++	−
mec1Δ tel1Δ sml1Δ	G_{25}-C	+++	+++	+++	−	+	+++
	G_{25}-D	+	+	+	−	+	+++
	G_{25}-H	+	+	−	−	+	+++
	G_{25}-I	+	+	−	−	+	+++
	G_{25}-L	+	+	+	−	+	+++
	G_{25}-M	+	+	+	−	+	+++
	G_{25}-O	+	+	+	−	+	+++
	G_{25}-P	+	+	+	−	+	+++
clb5Δ	G_{75}-A	+	+	+	+	+	+++
	G_{75}-B	+++	+++	+++	+++	+++	+
	G_{75}-C	+++	+++	+++	+++	+++	+++
	G_{75}-D	+++	+++	+++	+++	+++	+++
mre11Δ	G_{75}-A	+++	+++	+++	+++	+++	+++
	G_{75}-B	+++	+++	+++	+++	+++	+++
	G_{75}-C	+++	+++	+++	+	+++	+++
	G_{75}-D	+++	+++	+++	+	+++	−

+++, +, and − correspond to normal growth (WT level), reduced growth, and no growth on the corresponding medium, respectively.

*The letter and the number correspond to the name of the line and to the number of passages it went through, respectively.

[†]1% yeast extract, 2% (wt/vol) peptone, 2% (wt/vol) D-glucose.

[‡]1% yeast extract, 2% (wt/vol) peptone, 3% (wt/vol) glycerol.

[§]0,17% YNB w/o AA and AS, 0,5% ammonium sulfate, 2% (wt/vol) D-glucose, dropout powder as required. Growth was tested on the following media: SC-adenine, SC-arginine, SC-histidine, SC-leucine, SC-tryptophan, SC-uracil, SC-lysine, and SC-methionine.

[¶]Qualitatively assayed by crossing with testers strains (*MATa his1* and *MATα his1* strains).

Table S3. Location and nature of the minisatellite size variations observed in the MA lines

Minisatellite	Localization	Number of motifs	Motif size (bp)	MA lines: WT	MA lines: rad27Δ	MA lines: msh2Δ	MA lines: tsa1Δ
CYC8	Chr II 463757–463935	11	18	—	G_{100}-U: expansion (gain of 6 motifs)		
NUM1	Chr IV 757379–759782	13	192	—	G_{100}-S: contraction (loss of 5–6 motifs)	G_{100}-D: contraction (loss of 3 motifs)	G_{100}-B: contraction (loss of 4 motifs)
					G_{100}-U: contraction (loss of 9–10 motifs)		
HKR1	Chr IV 1307331–1308128	19	42	—	G_{100}-Q: contraction (loss of 4–5 motifs)	G_{100}-D: expansion (gain of 6 motifs)	G_{100}-A: contraction (loss of 9–10 motifs)
					G_{100}-S: contraction (loss of 4–5 motifs)		G_{100}-D: contraction (loss of 6–7 motifs)
					G_{100}-T: contraction (loss of 4–5 motifs)		
					G_{100}-U: contraction (loss of 2–3 motifs)		
YIL169c	Chr IX 25310–25856	17	42	—	G_{100}-Q: contraction (loss of 11 motifs)	G_{100}-B: contraction (loss of 1 motif)	G_{100}-B: contraction (loss of 10 motifs)
							G_{100}-D: expansion (gain of 1 motif)
MUC1	Chr IX 391078–392752	42	36–45	—	G_{100}-Q: contraction (loss of 16–17 motifs)		G_{100}-C: contraction (loss of 23–24 motifs)
(FLO11)					G_{100}-S: contraction (loss of 23–24 motifs)		G_{100}-D: contraction (loss of 23–24 motifs)
					G_{100}-T: contraction (loss of 23–24 motifs)		
					G_{100}-U: contraction (loss of 35–36 motifs)		
YMR317w	Chr XIII 908149–909052	25	36	—	G_{100}-Q: expansion (gain of 2 motifs)		G_{100}-A: expansion (gain of 16–17 motifs)
					G_{100}-S: expansion (gain of 2 motifs)		

Minisatellite size variation was determined by PCR with oligonucleotides designed in the flanking regions of the minisatellite.

Table S4. Aneuploidies observed in the MA lines

Strain	Line*	Aneuploidy	
		Disomic	Trisomic
tsa1Δ	G_{100}-D	III	
msh2Δ	G_{100}-A	III	
mec1Δ tel1Δ sml1Δ	G_{25}-D	III†	
	G_{25}-H	II†, X†	
	G_{25}-I	II†	
	G_{25}-L	XI†, XII†	
	G_{25}-M	III†	
	G_{25}-O	II†, XI†, XII†	
	G_{25}-P	XI†, XII†	
clb5Δ	G_{100}-A	I†, VIII	III†, IX
	G_{100}-B	III†, VII, XI	
	G_{100}-C	V†	
	G_{100}-D		III†
mre11Δ	G_{75}-B	I	
	G_{75}-C	XI	
	G_{75}-D	I	

*Strain name, line, and bottleneck passages as in Table 2. The chromosome copy number was determined by analyzing the read depth coverage from the NGS data and by aCGH.

†These chromosomes were involved in the mosaic aneuploidy phenomenon (main text and Fig. 3*A*).

Table S5. Chromosome copy number variations in the *mec1Δ tel1Δ sml1Δ* O line between the G_{24} to G_{26} bottlenecks

Colony	Chromosome copy number																
												XII					
	I	II	III	IV	V	VI	VII	VIII	IX	X	XI	1–450,000	490,000–1,065,000	XIII	XIV	XV	XVI
G_{24} colony	0.93	1.01	0.97	1.06	1.14	0.92	1.07	0.97	0.88	0.98	1.59	1.44	1.28	1.03	1.00	1.04	1.05
G_{25} colony	1.07	1.44	0.93	1.01	1.02	1.01	1.03	0.99	0.91	0.96	1.76	1.75	1.46	1.02	1.01	1.01	1.01
G_{26} colony 1	0.94	1.07	0.96	1.06	1.01	0.94	1.06	0.96	0.92	1.07	1.55	1.24	1.16	1.00	1.06	1.04	1.03
G_{26} colony 2	0.97	1.02	0.98	1.04	1.03	0.92	1.06	1.00	0.93	0.98	1.71	1.68	1.25	1.01	0.99	1.03	1.02
G_{26} colony 3	0.98	1.71	0.93	1.04	1.02	0.95	1.04	0.97	0.89	1.08	1.73	2.10	1.42	1.02	1.00	1.03	1.02
G_{26} colony 4	1.04	1.00	0.97	1.01	1.03	0.94	1.03	0.97	0.97	0.96	1.78	1.83	1.24	1.01	1.00	1.01	1.02
G_{26} colony 5	0.98	1.64	0.92	0.96	0.99	0.93	1.00	0.89	1.41	0.92	1.65	1.76	1.29	0.95	0.93	0.96	0.95
G_{26} colony 6	1.00	1.67	0.94	0.98	1.01	0.95	1.02	0.91	1.44	0.94	1.68	1.80	1.32	0.97	0.95	0.98	0.97
G_{26} colony 7	1.26	0.99	1.07	0.98	1.00	1.08	1.00	0.94	0.90	0.93	1.03	1.96	1.15	0.99	0.96	0.98	0.97
G_{26} colony 8	1.16	1.66	1.05	0.98	1.01	1.08	1.00	0.93	0.88	0.94	1.75	1.96	1.27	0.99	0.97	0.99	0.97
G_{26} colony 9	0.93	1.82	0.97	1.07	1.03	0.92	1.07	0.97	0.89	1.02	1.83	1.89	1.41	1.04	1.02	1.04	1.03
G_{26} colony 10	1.20	1.36	1.04	1.01	1.00	1.05	1.01	0.93	0.87	0.93	1.82	1.87	1.37	0.98	0.98	0.98	0.98

The chromosome copy number was determined after 24, 25, and 26 colonies bottlenecks using aCGH.

Other Supporting Information Files

Dataset S1 (XLS)
Dataset S2 (XLS)
Dataset S3 (XLS)
Dataset S4 (XLS)
Dataset S5 (XLS)
Dataset S6 (XLS)
Dataset S7 (XLS)
Dataset S8 (XLS)
Dataset S9 (XLS)
Dataset S10 (XLS)